https://doi.org/10.5194/egusphere-2026-4285
Preprint. Discussion started: 19 August 2026

Impact of GNSS zenith total delay and tropospheric gradient Assimilation on severe weather: a case study of Super Typhoon Koinu

Rohith Thundathil[1,2], Florian Zus[2], Thomas Schwitalla[3], Galina Dick[2], Jens Wickert[1,2]

[1]Institute of Geodesy and Geoinformation Sciences, Technische Universität, Berlin, Kaiserin-Augusta-Allee 104 10553 Berlin, Germany
[2]Section 1.1 Space Geodetic Techniques, GFZ Helmholtz Centre for Geosciences, Telegrafenberg, 14473 Potsdam, Germany
3Institute of Physics and Meteorology, University of Hohenheim, Garbenstrasse 30, 70599 Stuttgart,Germany

Correspondence to: Rohith Thundathil (r.thundathil@tu-berlin.de)

Abstract. In this study, we investigate the impact of assimilating Global Navigation Satellite System (GNSS) Zenith Total Delays (ZTDs) and tropospheric gradients (TGs) on the simulation of Super Typhoon Koinu (2023) using the Weather Research and Forecasting (WRF) model. Four data assimilation experiments are conducted: a control experiment assimilating conventional observations only, experiments separately assimilating ZTDs and tropospheric gradients on top of conventional observations, and a combined experiment assimilating both ZTDs and tropospheric gradients on top of the conventional observations. A two-month assimilation experiment using observations from approximately 250 GNSS stations demonstrates the overall benefit of GNSS data, with reductions in root-mean-square error (RMSE) of up to 60 % in ZTD when both ZTDs and tropospheric gradients are assimilated. Assimilation of tropospheric gradients alone also reduces the ZTD RMSE, demonstrating that gradients provide independent and complementary information beyond the vertically integrated moisture constraint of ZTDs. The impact of Typhoon Koinu is then examined as it approaches Taiwan between 3 and 6 October 2023. Continuous assimilation of GNSS observations improves the representation of the atmospheric moisture field surrounding the cyclone, leading to changes in the spatial distribution of integrated water vapor and the azimuthal moisture asymmetry around the storm. These moisture adjustments produce small but systematic improvements in the environmental deep-layer steering flow and, consequently, modest reductions in typhoon track error after landfall over Taiwan. The combined assimilation of ZTDs and tropospheric gradients also provides the most accurate simulation of cyclone intensity. The results demonstrate that tropospheric gradients complement ZTDs by improving the representation of horizontal moisture variability, thereby enhancing the simulation of the tropical cyclone environment. This study highlights the potential of assimilating multiple GNSS tropospheric products to improve tropical cyclone prediction in numerical weather prediction systems.

1 Introduction

Global Navigation Satellite Systems (GNSS) are essential in modern society, supporting positioning, navigation, and timing applications for various civilian and commercial activities. Beyond these well-established applications, GNSS observations have become increasingly important in geosciences, providing valuable information on atmospheric, surface, and geophysical

https://doi.org/10.5194/egusphere-2026-4285
Preprint. Discussion started: 19 August 2026

processes. GNSS-based techniques enable the monitoring of atmospheric water vapor, land surface properties, and crustal deformation with high accuracy and continuity, offering unique insights into Earth system dynamics (Wickert et al., 2020). GNSS meteorology uses the time delay of radio signals traveling from the satellite to the receiver station to monitor atmospheric water vapor. Zenith Total Delay (ZTD) is a key measurement in GNSS meteorology (Bevis et al., 1992), closely linked to the Integrated Water Vapor (IWV) above the station. Over Europe, GNSS-derived ZTD observations are available in near real time (NRT) from several station networks, such as the European Meteorological Network Global Navigation Satellite Systems Water Vapor Program (EGVAP). Assimilation studies have demonstrated that ZTD observations improve forecast skill (Vedel and Huang, 2004). Consequently, GNSS ZTD observations are assimilated operationally at several European weather services (Poli et al., 2007; Yan et al., 2009; Boniface et al., 2009; Bennitt & Jupp, 2012; Lindskog et al., 2017; Rohm et al., 2019; Giannaros et al., 2020; Caldas-Alvarez and Khodayar, 2020). More recent studies further demonstrated the benefits of GNSS-derived atmospheric observations. Lagasio et al. (2019), Singh et al. (2019), Mascitelli et al. (2019, 2021), Yang et al. (2020), and Risanto et al. (2021) reported improvements in humidity, wind, temperature, and water vapor forecasts, with enhanced heavy rainfall prediction achieved through the combined assimilation of GNSS ZTD and radar observations (Yang et al., 2020).

When considering GNSS data products, moisture information via ZTDs is currently operational; however, it provides limited atmospheric information. For a new observation type to be valuable in data assimilation, it must contribute information that is not already contained in existing observing systems. Bennitt and Jupp (2012) and Mahfouf et al. (2015) pointed out that the limitations of ZTD stem from its inability to offer insights into the changes or gradients in moisture. This information is hidden in two other types of observations: Tropospheric Gradients (TGs) and Slant Total Delays (STDs). Tropospheric gradients (Bar-Sever et al., 1998) describe directional variations in atmospheric delay and therefore provide information on the horizontal variability of atmospheric moisture in the lower troposphere. Estimated TGs have been shown to correspond closely to atmospheric moisture patterns observed by water vapor radiometers. Several studies have assessed the ability of TGs to represent horizontal moisture variability. For example, Iwabuchi et al. (2003) found a strong correlation between these TGs and moisture field gradients: typically, TGs point from dry to moist regions. Douša et al. (2016) analyzed data from hundreds of stations in central Europe and confirmed that TGs reflect real tropospheric features. Kačmařík et al. (2019) emphasized the sensitivity of TGs to processing models, noting that the accuracy of real-time products depends on high-quality GNSS orbits and clocks. Walpersdorf et al. (2001) validated TGs using the ALADIN model, while Brenot et al. (2013) demonstrated their ability to capture moisture variations associated with deep convection. Li et al. (2015) reported that improved satellite observation geometry enhances TG estimation, and Morel et al. (2015) confirmed the consistency of TG estimates obtained using different processing software.

While ZTD has been widely assimilated into operational NWP models, the use of TGs has remained largely confined to diagnostic and validation studies until recently. One of the main challenges is the development of observation operators (Zus et al., 2019). Recently, Zus et al. (2023) developed an efficient operator for TGs, and Thundathil et al. (2024) implemented it in the Weather Research and Forecasting (WRF) model data assimilation system. Recent assimilation experiments combining

https://doi.org/10.5194/egusphere-2026-4285
Preprint. Discussion started: 19 August 2026

ZTDs and TGs have demonstrated improvements in the representation of atmospheric moisture fields (Thundathil et al., 2024). In a recent sensitivity study, it was found that assimilating TGs in addition to ZTDs from a sparse (1-degree) station network yields an improvement equivalent to that from assimilating only ZTDs from a dense (0.5-degree) station network (Thundathil et al., 2025). These findings suggest that TGs can partially compensate for sparse observational coverage by providing additional information on horizontal moisture variability.

Although previous studies have demonstrated the potential benefits of assimilating tropospheric gradients, their impact has primarily been evaluated in midlatitude environments. The effectiveness of TG assimilation in tropical regions characterized by high atmospheric moisture content and strong mesoscale variability has received little attention. In particular, it is not yet clear whether the additional horizontal moisture information provided by TGs can improve the representation of the moisture field surrounding tropical cyclones, thereby influencing storm prediction.

These developments motivate the use of GNSS-derived tropospheric gradients in high-impact weather forecasting. Tropical cyclones (referred to as typhoons in the western North Pacific) are particularly sensitive to the surrounding atmospheric moisture distribution and environmental circulation. The spatial structure of atmospheric moisture influences convective organization, diabatic heating, and the surrounding large-scale flow that governs storm motion. Because tropospheric gradients contain information on horizontal moisture variability, they may help improve the representation of asymmetric moisture structures that play an important role in tropical cyclone evolution and motion.

In this study, we investigate the impact of assimilating GNSS ZTDs and TGs on the simulation of Super Typhoon Koinu (2023) using the WRF model. The objectives of this study are threefold. First, we assess the impact of assimilating GNSS tropospheric gradients in the moisture-rich western North Pacific. Second, we investigate how GNSS observations modify the spatial distribution and asymmetry of atmospheric moisture surrounding Typhoon Koinu. Third, we examine whether these moisture changes affect the environmental steering flow and, consequently, the simulated storm track.

To complement the detailed typhoon case study, a two-month assimilation experiment using observations from approximately 250 GNSS stations was conducted. This statistical evaluation enables the robustness of the assimilation impact to be assessed under a wide range of meteorological conditions. To our knowledge, this is one of the first studies to investigate the impact of assimilating GNSS tropospheric gradients on the simulation and prediction of a tropical cyclone in the western North Pacific. The study therefore provides both a statistical assessment of the observational impact and a process-oriented analysis of the mechanisms through which GNSS observations influence tropical cyclone prediction.

The paper is structured as follows:

Section 2 outlines the retrieval methods for GNSS ZTDs and tropospheric gradients used in this study. Section 3 details the model setup, including data and experimental design, and Section 4 examines the influence of GNSS observations on atmospheric moisture, environmental steering flow, and typhoon track prediction. Section 5 summarizes the key findings and discusses their implications for future numerical weather prediction applications.

https://doi.org/10.5194/egusphere-2026-4285
Preprint. Discussion started: 19 August 2026

2. GNSS Zenith Total Delays and Tropospheric Gradients

As GNSS signals propagate through the neutral atmosphere, they experience a propagation delay that depends on the atmospheric refractive index. In GNSS data analysis, this delay is parameterized using mapping functions together with zenith delay and horizontal gradient components. The total tropospheric delay, T, at a receiver is expressed as a function of the satellite elevation angle e and azimuth angle a:

$$T(e,a) = m_h(e) . Z_h + m_w(e) . Z_w + m_g(e) [\cos(a) . NG + \sin(a) . EG] \quad (1)$$

where Z_h and Z_w denote the zenith hydrostatic delay (ZHD) and zenith wet delay (ZWD), respectively, while NG and EG are the north and east tropospheric gradient components. The hydrostatic, wet, and gradient mapping functions are represented by m_h, m_w, and m_g, respectively. The ZTD is the sum of the hydrostatic and wet components,

$$ZTD = Z_h + Z_w. \quad (2)$$

The WRF Data Assimilation (WRFDA) system already includes a forward operator together with its tangent-linear and adjoint counterparts for ZTD assimilation. The simulated ZTD is obtained by vertically integrating the atmospheric refractivity,

$$ZTD = 10^{-6} \int \mathrm{N}\, dz \quad (3)$$

where the refractivity N is a function of pressure, temperature, and humidity (Thayer, 1974), with z denoting the height above the receiver station. During GNSS processing, ZTD together with the north (NG) and east (EG) tropospheric gradient components are estimated simultaneously with the geodetic parameters using a least-squares adjustment (Gendt et al., 2004). Because these quantities depend on the atmospheric state above and around the station, they are treated as atmospheric observations in the data assimilation system. The three quantities, depending on the state of the atmosphere in the vicinity of the station, are considered observations. The forward operator for tropospheric gradients follows the efficient formulation proposed by Zus et al. (2023). At each station location, the north and east gradient components are computed from the horizontal gradients of atmospheric refractivity using a closed-form expression derived from Davis et al. (1993):

$$NG = 10^{-6} \int z\mathrm{N}_y\, dz \quad (4)$$

$$EG = 10^{-6} \int z\mathrm{N}_x\, dz \quad (5)$$

Here, x, y, and z represent the Cartesian coordinates and partial derivatives are denoted by the corresponding subscripts. As for ZTD, the gradient components are evaluated by numerical integration through the atmospheric column.

The tropospheric gradient operator developed by Zus et al. (2023) was implemented in WRFDA version 4.4.1 by Thundathil et al. (2024). Initial data assimilation experiments over Germany demonstrated that assimilating tropospheric gradients together with ZTD observations improves the representation of atmospheric moisture fields. For diagnostic purposes, the open-source ray-tracing software developed by Zus et al. (2025) was used to compute simulated ZTDs and tropospheric gradients directly from WRF output, enabling a consistent comparison between model-simulated and observed GNSS products.

https://doi.org/10.5194/egusphere-2026-4285
Preprint. Discussion started: 19 August 2026

Unlike ZTD, which represents the vertically integrated atmospheric delay, tropospheric gradients are sensitive to the horizontal variability of atmospheric refractivity. Consequently, ZTD and tropospheric gradients provide complementary information on the atmospheric moisture field, making their combined assimilation potentially beneficial for numerical weather prediction.

3. Model setup

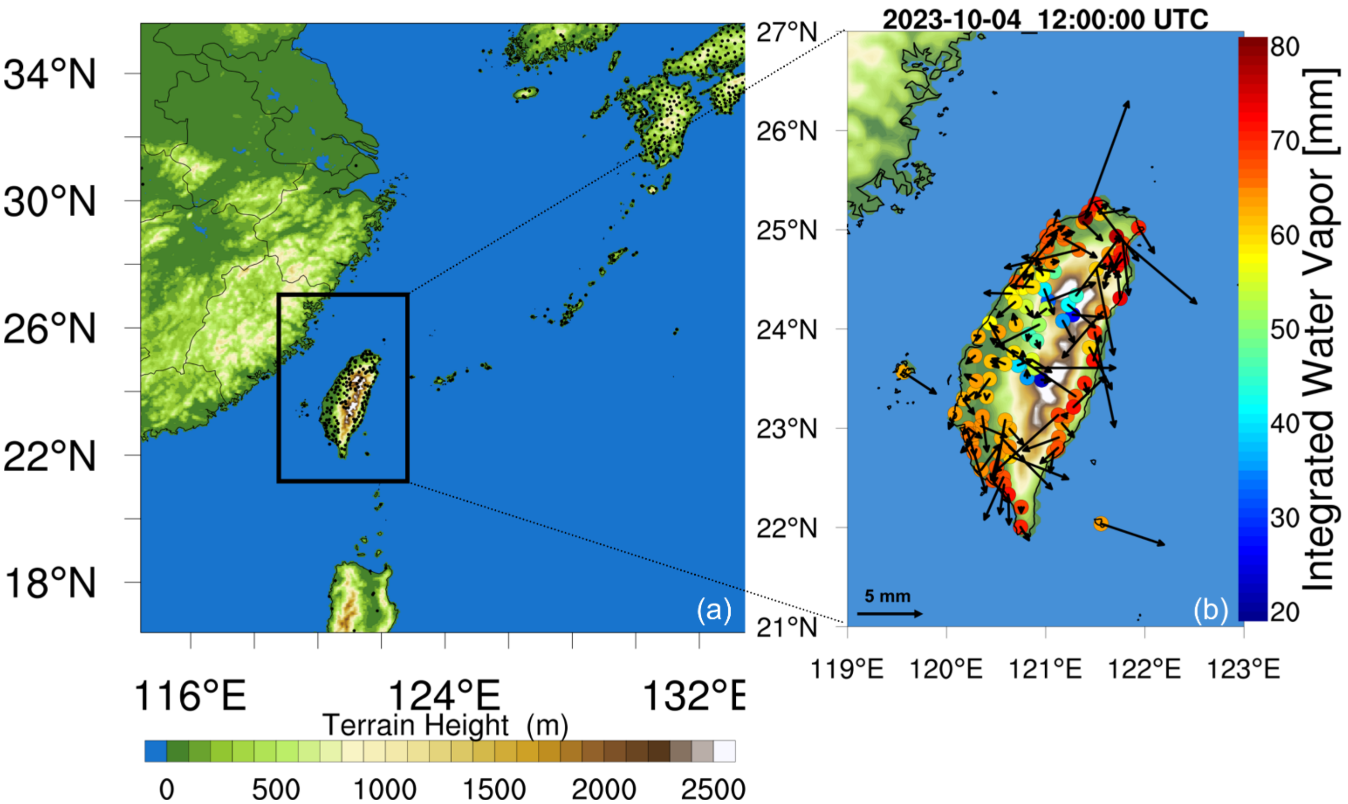

Figure 1 (a) WRF model domain used in this study. Terrain height (m) is shown by the shaded colors, and black dots indicate the locations of the approximately 250 ground-based GNSS stations assimilated during the experiments. (b) Zoomed view of Taiwan at 1200 UTC on 4 October 2023, showing the IWV (mm) derived from GNSS observations. Black arrows represent the estimated tropospheric gradient vectors.

In this study, the Weather Research and Forecasting (WRF) model version 4.4.1 was employed with the Advanced Research WRF (ARW) dynamical core (Skamarock et al., 2008). WRF is a widely used mesoscale numerical weather prediction system for both research and operational forecasting worldwide (Powers et al., 2017).

The WRF model was configured over a single regional domain comprising 400 × 400 horizontal grid points with a horizontal grid spacing of 0.05° (approximately 5.6 km), resulting in a domain size of approximately 2220 × 2220 km². The domain was centered at 26° N and 124° E and covers the western North Pacific, including Taiwan, the Ryukyu Islands, and southeastern China (Fig. 1a). This setup represents a tropical-to-subtropical environment strongly influenced by monsoon circulation and

https://doi.org/10.5194/egusphere-2026-4285
Preprint. Discussion started: 19 August 2026

tropical cyclone activity. A horizontal grid spacing of approximately 5.6 km was selected to balance computational efficiency with the long simulation period required for the two-month assimilation experiment. This configuration enabled multiple assimilation experiments to be performed while maintaining sufficient resolution to represent the large-scale moisture distribution and tropical cyclone environment. Future work will investigate the impact of GNSS observations using convection-permitting simulations. A Cylindrical Equidistant (latitude–longitude) map projection was used for the domain configuration. The model was configured with 50 vertical levels extending from the surface to the model top at approximately 50 hPa, using a hybrid terrain-following vertical coordinate with fine resolution in the lower tropospheric levels near the surface. The model time step was set to 20 s, with radiation called every 5 minutes. The simulation started on 1 September 2023 at 00 UTC. Initial and lateral boundary conditions were obtained from the ECMWF operational analysis with a horizontal resolution of approximately 9 km and updated every 6 h. Figure 1a shows the model domain together with the distribution of GNSS stations used in the assimilation experiments. The inset (Fig. 1b) highlights the dense GNSS network over Taiwan, where IWV and tropospheric gradients are available during the landfall of Typhoon Koinu.

The physical parameterizations used in the WRF simulations are summarized in Table 1. They include the Thompson aerosol-aware microphysics scheme, RRTMG longwave radiation, Dudhia shortwave radiation, the YSU planetary boundary layer scheme, the revised MM5 Monin–Obukhov surface layer scheme, the Noah land surface model, and the Grell–Freitas scale-aware cumulus parameterization. The selected physics options have been widely used for tropical cyclone simulations in the WRF model and provide a suitable representation of cloud microphysics, boundary-layer processes, land–atmosphere interactions, and convection. Because the horizontal grid spacing (5.6 km) lies within the gray zone of convection, the scale-aware Grell–Freitas cumulus parameterization was employed to represent unresolved convective processes.

Table 1 Physical parameterization schemes used in the WRF model configuration.

Model component	Parameterization scheme
Microphysics	Thompson aerosol-aware double-moment scheme (Thompson et al., 2008)
Longwave radiation	Rapid Radiative Transfer Model for GCMs (RRTMG; Iacono et al., 2008)
Shortwave radiation	Dudhia scheme (Dudhia, 1989)
Planetary boundary layer	Yonsei University (YSU) scheme (Hong et al., 2006)
Surface layer	Revised MM5 Monin–Obukhov scheme (Jiménez et al., 2012)
Land surface	Noah Land Surface Model (Noah LSM; Chen and Dudhia, 2001)
Cumulus parameterization	Grell–Freitas scale-aware ensemble scheme (Grell and Freitas, 2014)

3.1 Data

For the assimilation experiments, GNSS tropospheric products from approximately 250 stations were obtained from the Nevada Geodetic Laboratory (http://geodesy.unr.edu/). The spatial distribution of the stations is shown in Fig. 1a. To account for systematic differences between the model and the observations, station-specific bias corrections were applied to both GNSS

https://doi.org/10.5194/egusphere-2026-4285
Preprint. Discussion started: 19 August 2026

ZTD and tropospheric gradients following the methodology of Thundathil et al. (2024). The bias corrections were derived from two months of control simulations and subsequently applied throughout the assimilation experiments.

The observation error assigned to GNSS ZTD observations in operational numerical weather prediction typically ranges from 5 to 15 mm. In a previous study over central Europe, Thundathil et al. (2025) adopted observation errors of 8 mm for ZTD and 0.65 mm for tropospheric gradients. Because of the larger spatial and temporal variability of atmospheric moisture over the tropical and subtropical western North Pacific, a larger observation error was adopted for ZTD in this study. Observation errors for the north and east tropospheric gradient components were estimated from the standard deviation of the observation-minus-background (O–B) statistics obtained from the control experiment. Since the O–B statistics include contributions from both observation and background errors, a conservative observation error of 1 mm was applied to both gradient components to avoid over-constraining the analysis.

To supplement the GNSS observations, a complete set of conventional observations was included throughout the two-month study period, as detailed in Table 2. A spatial map of the observations is shown in Fig. 2.

Table 2 Conventional and GNSS observations assimilated every 3 hours.

Observation type	Average number per assimilation cycle
SYNOP	393
METAR	82
Ship	47
Buoy	41
TEMP (radiosondes)	16
AMDAR	700
TAMDAR	2,150
GNSS stations	~250

Conventional observations primarily constrained the atmospheric temperature, wind, and pressure fields, whereas GNSS observations provided complementary information on atmospheric moisture distribution via ZTD and tropospheric gradient measurements. Each GNSS station contributes one ZTD observation and two tropospheric gradient components (north and east) at every assimilation cycle. All conventional and GNSS observations were assimilated sequentially using a three-hour cycling interval throughout the two-month experiment. The three-hour assimilation interval was chosen to match the temporal availability of conventional observations while allowing high-frequency GNSS observations to constrain the evolving atmospheric moisture field continuously.

https://doi.org/10.5194/egusphere-2026-4285
Preprint. Discussion started: 19 August 2026

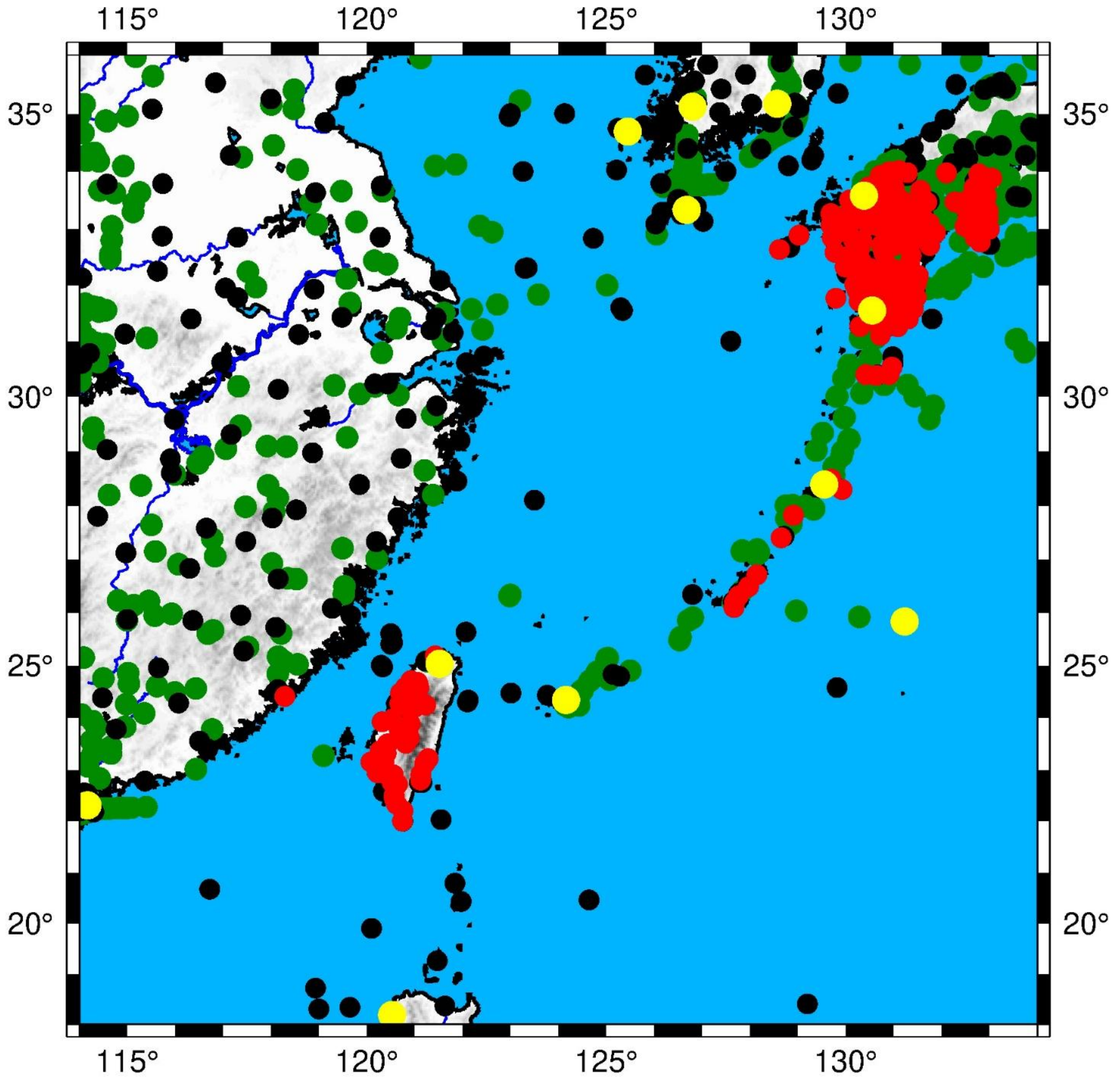

185 **Figure 2 Spatial distribution of the observations assimilated every 3 h during the experiments. Red circles denote the approximately 250 ground-based GNSS stations providing ZTDs and tropospheric gradients. Green circles indicate surface observations (SYNOP/METAR), yellow circles denote radiosonde (TEMP) stations, and black circles represent marine and aircraft observations (ship, buoy, AMDAR, and TAMDAR).**

https://doi.org/10.5194/egusphere-2026-4285
Preprint. Discussion started: 19 August 2026

3.2 DA Framework

Data assimilation was performed using the deterministic three-dimensional variational (3DVAR) data assimilation system implemented in WRFDA version 4.4.1. The analysis is obtained by minimizing a cost function that balances the background state with the available observations, weighted by their respective error statistics. The 3DVAR cost function equation is given by

$$J(x) = \frac{1}{2}(x - x_b)^T \mathbf{B}^{-1}(x - x_b) + \frac{1}{2}(y - \mathbf{H}(x))^T \mathbf{R}^{-1}(y - \mathbf{H}(x)) \tag{6}$$

Here, x denotes the analysis state vector, x_b the background (first guess), and y the observation vector. The observation operator **H** maps the model variables into observation space. The matrices **B** and **R** represent the background and observation error covariance matrices, respectively. Following the standard 3DVAR formulation, observation errors are assumed to be uncorrelated, and **R** is therefore specified as a diagonal matrix. A climatological background error covariance matrix was estimated using the National Meteorological Center (NMC) method (Parrish and Derber, 1992), in which forecast error statistics are approximated from differences between 24-h and 12-h forecasts. The statistics were derived from forecasts during September 2023 and subsequently used throughout the assimilation experiments. The CV5 control-variable option was adopted because it provides independent control of moisture increments and minimizes cross-correlations between moisture and the remaining control variables. The corresponding control variables include stream function, unbalanced velocity potential, unbalanced temperature, pseudo-relative humidity, and unbalanced surface pressure.

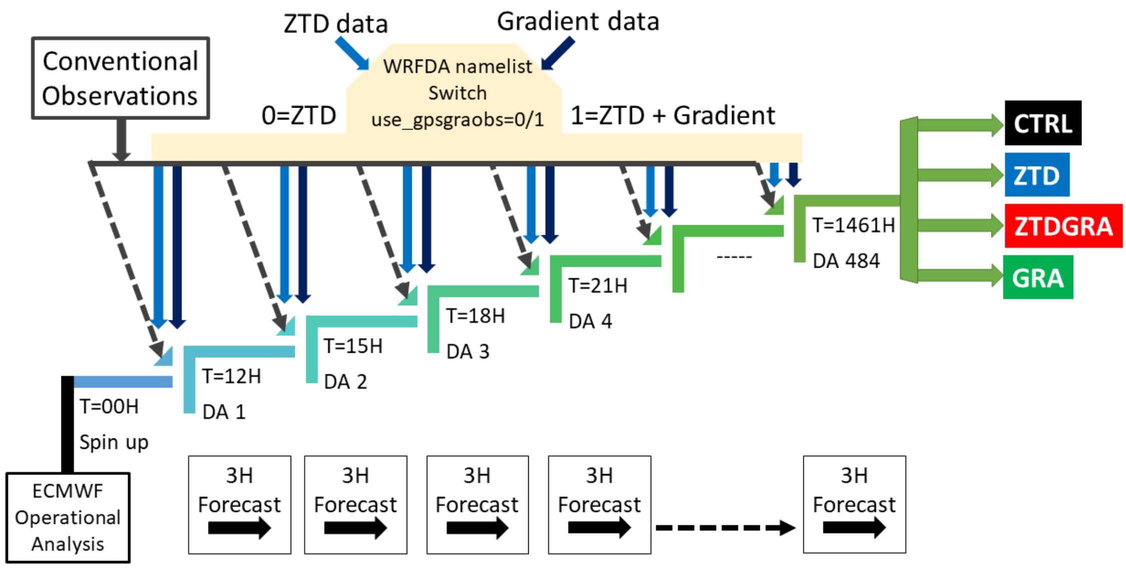

Figure 3 Schematic illustration of the WRF 3DVAR rapid-update-cycle data assimilation framework used in this study. The simulations are initialized from the ECMWF operational analysis and employ a 3-hour assimilation cycle throughout the two-month experiment. Conventional observations are assimilated in all experiments, while GNSS ZTDs and tropospheric gradients are assimilated according to the WRFDA namelist option use_gpsgraobs. Setting use_gpsgraobs = 0 enables assimilation of ZTD observations only, whereas use_gpsgraobs = 1 activates the simultaneous assimilation of both ZTDs and tropospheric gradients. Four experiments are performed: CTRL (conventional observations only), ZTD (CTRL + ZTD), GRA (CTRL + TG), and ZTDGRA (CTRL + ZTD + TG).

https://doi.org/10.5194/egusphere-2026-4285
Preprint. Discussion started: 19 August 2026

Four assimilation experiments were performed (Fig. 3). The CTRL experiment assimilated only conventional observations. The ZTD experiment additionally assimilated GNSS ZTDs, whereas the GRA experiment assimilated only GNSS tropospheric gradients, along with conventional observations. The ZTDGRA experiment assimilated both GNSS ZTD and tropospheric gradients simultaneously. Assimilation of tropospheric gradients was enabled through the newly implemented WRFDA namelist option use_gpsgraobs. Setting "use_gpsgraobs = 0" activates the standard ZTD-only configuration, whereas "use_gpsgraobs = 1" enables the assimilation of both ZTD and tropospheric gradients. Figure 3 illustrates our data assimilation approach.

The assimilation framework presented here extends the operational capabilities of WRFDA by incorporating GNSS tropospheric gradients alongside ZTDs. The complementary nature of these two observation types allows both the vertically integrated atmospheric moisture and its horizontal variability to be constrained within a consistent variational framework. The two-month cycling experiment and the Typhoon Koinu case study presented in the following sections provide a comprehensive evaluation of the information content of tropospheric gradients and their potential to improve numerical weather prediction in a moisture-rich tropical environment.

4 Results

4.1 Typhoon case overview and GNSS observation coverage

Super Typhoon Koinu developed over the western North Pacific in late September 2023 and intensified while moving westward toward the northern Philippines and the Luzon Strait. The storm subsequently turned northwestward and approached the southern coast of Taiwan in early October, reaching super-typhoon intensity before making landfall near the Hengchun Peninsula. After interacting with the complex terrain of southern Taiwan, the cyclone weakened as it continued westward toward the southeastern coast of China. The evolution of Koinu during this period provides an ideal opportunity to evaluate the impact of ground-based GNSS observations on tropical cyclone prediction, particularly during landfall when the storm moved within the coverage of a dense GNSS network.

The study region is characterized by complex terrain, with mountain ranges exceeding 2000 m over Taiwan and elevated terrain extending across parts of southeastern China. These topographic features strongly influence atmospheric circulation and moisture transport during typhoon events. Figure 1a shows the model domain, terrain elevation, and the spatial distribution of the GNSS stations used in this study. The network is particularly dense over Taiwan and the Ryukyu Islands, providing excellent observational coverage along the typhoon track.

The dense GNSS network provides high-frequency atmospheric observations that capture the rapid moisture changes associated with the approaching typhoon. The highest station density occurs over Taiwan, where the network is sufficiently dense to resolve mesoscale moisture gradients associated with the storm's outer rainbands and low-level inflow. In contrast, observational coverage over the open ocean is relatively sparse, as expected for ground-based GNSS observations. As Koinu

https://doi.org/10.5194/egusphere-2026-4285
Preprint. Discussion started: 19 August 2026

approached Taiwan, however, the storm entered a region with substantially improved observational coverage, allowing the evolving moisture field to be sampled in much greater detail.

The spatial relationship between the GNSS network and the storm track is central to this study. During landfall, the circulation of Koinu passed directly over the densely instrumented region of Taiwan, enabling the assimilation of a large number of GNSS ZTDs and tropospheric gradients. Together, these observations constrain both the vertically integrated atmospheric water vapor content and its horizontal variability, providing a more complete description of the moisture environment surrounding the storm. This unique observational configuration offers an excellent opportunity to evaluate the contribution of GNSS-derived atmospheric observations to predicting tropical cyclone structure and track. Before examining the Typhoon Koinu case in detail, the overall impact of GNSS data assimilation is first evaluated using the two-month assimilation experiment.

4.2 Impact of GNSS assimilation: two-month statistics

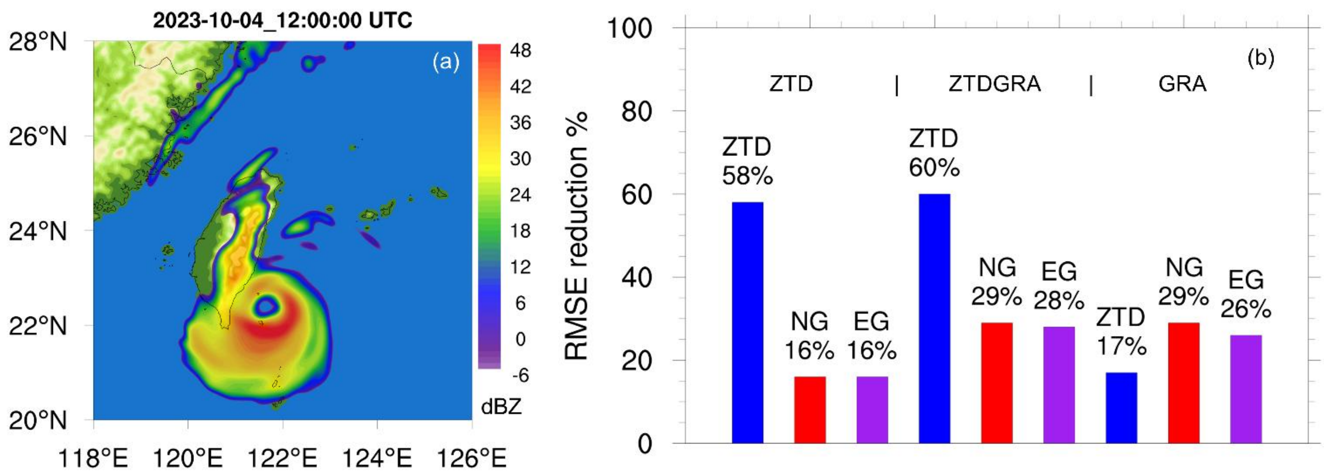

Figure 4 (a) Simulated maximum radar reflectivity (dBZ) at 12:00 UTC on 4 October 2023, illustrating the convective structure of Super Typhoon Koinu as it approached Taiwan. (b) Percentage reduction in root-mean-square error (RMSE) relative to the CTRL experiment from the two-month assimilation experiment (1 September–31 October 2023) using observations from approximately 250 GNSS stations. The bars show the RMSE reduction for ZTDs, north gradient (NG), and east gradient (EG) observations for the ZTD, ZTDGRA, and GRA experiments. The combined assimilation of ZTDs and tropospheric gradients (ZTDGRA) provides the largest overall improvement, demonstrating the complementary information content of the tropospheric gradients.

The simulated radar reflectivity field at 1200 UTC on 4 October 2023 (Fig. 4a) illustrates the convective structure of Super Typhoon Koinu as it approached Taiwan. The model reproduces a compact eyewall with reflectivity values exceeding 40 dBZ, surrounded by well-organized spiral rainbands extending toward the north and northwest of the storm center. These features indicate that the model captures the principal dynamical and thermodynamical characteristics of the storm prior to landfall. The simulation was initialized one month before the typhoon event as part of the continuous cycling experiment, demonstrating that the assimilation framework maintained a realistic large-scale atmospheric state throughout the study period.

The overall performance of the GNSS assimilation experiments is evaluated using two months of assimilation statistics from approximately 250 GNSS stations (Fig. 4b). The results are presented as percentage reductions in root-mean-square error (RMSE) relative to the CTRL experiment. Assimilating GNSS ZTD observations reduces the ZTD RMSE by approximately

https://doi.org/10.5194/egusphere-2026-4285
Preprint. Discussion started: 19 August 2026

58%, while also decreasing the RMSE of the north and east tropospheric gradients by about 16%. When both ZTD and tropospheric gradients are assimilated simultaneously (ZTDGRA), the ZTD RMSE reduction increases to approximately 60%, accompanied by reductions of about 29% and 28% for the north and east gradients, respectively. In contrast, the GRA experiment reduces the ZTD RMSE by approximately 17% and produces substantial reductions of about 29% and 26% for the north and east gradient components.

An important finding is that assimilating tropospheric gradients alone improves ZTD statistics, demonstrating that gradients contain independent atmospheric information rather than merely duplicating that in ZTD observa tions. The additional improvement achieved in the combined ZTDGRA experiment therefore reflects the complementary nature of the two GNSS observation types.

Overall, the two-month statistical evaluation demonstrates that GNSS observations consistently improve the atmospheric analysis. While ZTD observations primarily constrain the vertically integrated atmospheric moisture, tropospheric gradients provide complementary information on its horizontal variability. Their combined assimilation produces the largest improvement across all evaluated quantities, highlighting the benefit of jointly assimilating both observation types.

The consistency of these improvements over the two months indicates that the positive impact of tropospheric gradient assimilation is not limited to a single weather event but is robust across a range of meteorological conditions encountered during the study period. This provides a strong basis for examining the influence of GNSS observations during the evolution of Super Typhoon Koinu, which is analyzed in the following sections.

4.3 Impact of GNSS assimilation on atmospheric moisture analysis

To investigate how GNSS observations modify the moisture environment surrounding Typhoon Koinu, differences in IWV between the assimilation experiments and the control simulation were analyzed. Because IWV represents the vertically integrated atmospheric moisture content, it provides an effective measure of how GNSS observations modify the storm's large-scale moisture distribution.

https://doi.org/10.5194/egusphere-2026-4285
Preprint. Discussion started: 19 August 2026

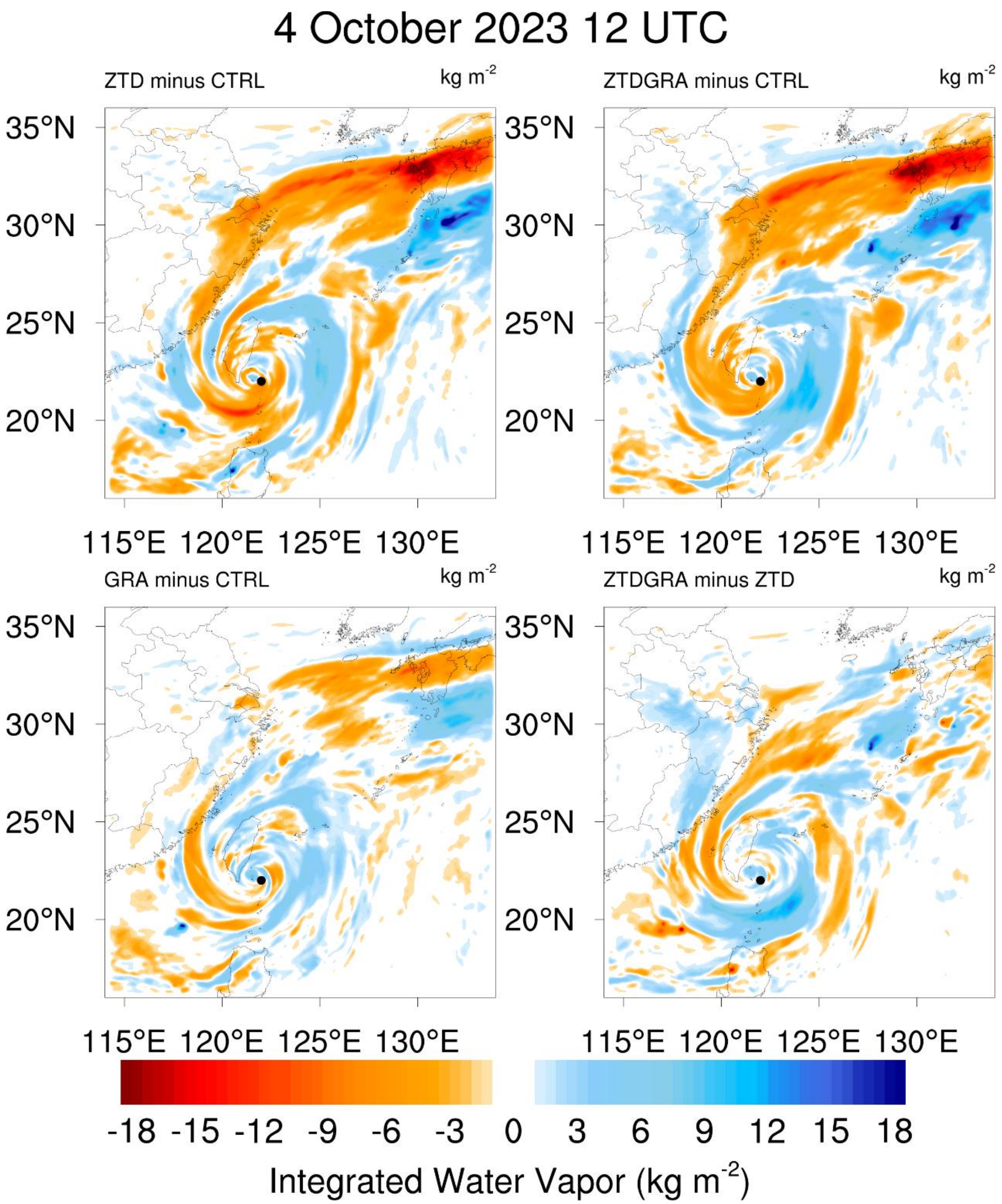

Figure 5 Differences in integrated water vapor (IWV; kg m^{-2}) at 12:00 UTC on 4 October 2023 resulting from the assimilation of GNSS observations during the approach of Super Typhoon Koinu to Taiwan. Panels show (a) ZTD − CTRL, (b) ZTDGRA − CTRL, (c) GRA − CTRL, and (d) ZTDGRA − ZTD. Warm colors (red) indicate reduced water vapor relative to the reference experiment, while cool colors (blue) indicate increased water vapor. The black dot denotes the best-track position of the typhoon center. The ZTD and ZTDGRA experiments produce pronounced moisture adjustments surrounding the cyclone, whereas the ZTDGRA − ZTD difference isolates the additional impact of assimilating tropospheric gradients, highlighting their contribution to refining the horizontal moisture distribution around the storm.

https://doi.org/10.5194/egusphere-2026-4285
Preprint. Discussion started: 19 August 2026

Figure 5 shows that assimilating GNSS observations systematically modifies the moisture distribution surrounding the typhoon. In the ZTD experiment (Fig. 5a), localized moistening is evident within the southeastern quadrant of the cyclone, where positive IWV anomalies of approximately 8–10 kg m^{-2} coincide with the primary low-level inflow and outer rainband region. At the same time, a broad region of reduced moisture develops north of the storm along the strong subtropical moisture gradient extending across approximately 32–35°N. These changes suggest that assimilating ZTD observations primarily adjusts the magnitude of the column-integrated moisture field while preserving the overall structure of the cyclone.

The combined ZTDGRA experiment (Fig. 5b) exhibits a similar large-scale pattern but with more coherent and spatially organized moisture adjustments. The moist anomalies within the southeastern inflow region become more concentrated and better aligned with the spiral rainbands identified in the simulated radar reflectivity (Fig. 4a). In contrast, the drying north of the cyclone becomes more sharply defined. These results indicate that assimilating tropospheric gradients improves the spatial organization of the moisture field by providing additional information on its horizontal variability.

Assimilating tropospheric gradients alone (Fig. 5c) produces smaller changes in the total column moisture than the ZTD experiment, consistent with the fact that gradients do not directly constrain the IWV content. Nevertheless, the GRA experiment modifies the spatial distribution of moisture, particularly around the storm periphery, demonstrating that tropospheric gradients primarily influence the horizontal organization of the atmospheric moisture field rather than its overall magnitude.

The direct contribution of tropospheric gradients is illustrated by the difference between the ZTDGRA and ZTD experiments (Fig. 5d). Although the magnitude of the IWV differences is modest, the additional moistening and drying occur in a distinctly asymmetric pattern around the cyclone, particularly within the southeastern inflow sector and along the outer rainbands. Additional drying north and northwest of the storm further indicates that tropospheric gradients refine the representation of horizontal moisture contrasts that are not fully constrained by ZTD observations alone.

Overall, the GNSS assimilation experiments demonstrate that ZTD and tropospheric gradients play complementary roles in the moisture analysis. While ZTD observations primarily adjust the total atmospheric moisture content, tropospheric gradients refine its horizontal distribution, resulting in a more physically consistent representation of the moisture field surrounding the cyclone. Because the surrounding moisture environment strongly influences tropical cyclone intensity and motion, these changes provide a physical basis for the subsequent analyses of moisture asymmetry, environmental steering flow, and track evolution.

https://doi.org/10.5194/egusphere-2026-4285
Preprint. Discussion started: 19 August 2026

4.4 Contribution of tropospheric gradients to moisture asymmetry representation

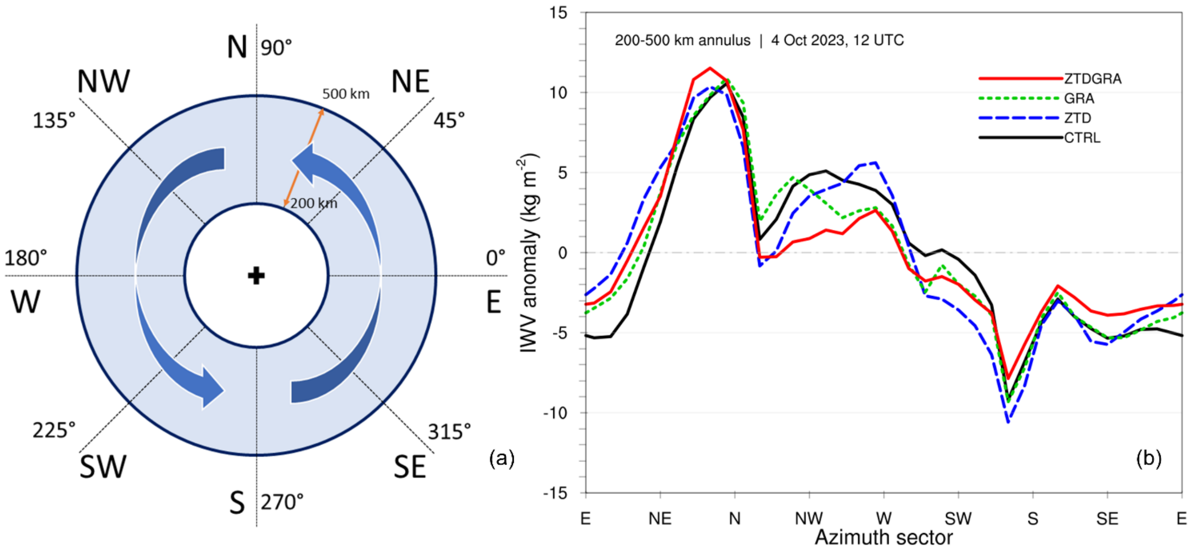

Figure 6 (a) Schematic illustrating the methodology used to quantify the azimuthal distribution of IWV around Typhoon Koinu. IWV values are sampled within an annular region extending from 200 to 500 km from the best-track storm center and averaged within successive azimuthal sectors measured clockwise from east. This approach isolates the environmental moisture distribution while minimizing the influence of the typhoon inner core. (b) Azimuthal distribution of IWV anomalies (kg m^{-2}) at 12:00 UTC on 4 October 2023 for the CTRL, ZTD, GRA, and ZTDGRA experiments. Assimilating GNSS observations modifies the directional distribution of atmospheric moisture surrounding the cyclone, while the inclusion of tropospheric gradients produces additional changes in the horizontal moisture asymmetry relative to the ZTD-only experiment.

The IWV difference fields shown in Fig. 5 indicate that GNSS assimilation modifies the spatial distribution of atmospheric moisture surrounding Typhoon Koinu. To further quantify these changes, the azimuthal distribution of IWV anomalies was analyzed within a radial annulus extending from 200 to 500 km from the storm center (Fig. 6a). This annulus samples the moisture environment outside the inner core while excluding the nearly axisymmetric eyewall region. For each experiment, IWV was averaged within successive azimuthal sectors, and the azimuthal mean was removed to isolate the asymmetric component of the moisture distribution.

Figure 6b shows a pronounced azimuthal moisture asymmetry in all experiments. Positive IWV anomalies dominate the northern part of the storm environment, reaching approximately 10–12 kg m^{-2}, whereas negative anomalies occur predominantly from the southwest through the southeast, with the strongest drying near the southern sector. The similarity of this broad pattern among the experiments indicates that the large-scale moisture asymmetry is already represented in the CTRL simulation. However, assimilation of the different GNSS products modifies both the magnitude and azimuthal structure of these anomalies.

https://doi.org/10.5194/egusphere-2026-4285
Preprint. Discussion started: 19 August 2026

The ZTD experiment produces noticeable changes relative to CTRL. In the eastern and northeastern sectors, the negative anomalies are reduced, while the positive anomaly around the northern sector is slightly enhanced. Farther west, ZTD maintains relatively strong positive anomalies between the northwest and west sectors. The largest difference occurs toward the south, where the ZTD experiment produces the strongest negative IWV anomaly among the four simulations, reaching approximately −10 kg m^{-2}. These changes are consistent with the strong constraint imposed by ZTD observations on the vertically integrated atmospheric moisture content.

The influence of tropospheric gradients is evident when the GRA and ZTDGRA experiments are compared with CTRL and ZTD. Assimilating gradients alone modifies the azimuthal moisture distribution without strongly changing its overall north–south structure. In particular, GRA reduces the positive anomalies over parts of the northwest and western sectors relative to CTRL and ZTD and modifies the magnitude of the southern moisture deficit. This behavior is consistent with the nature of tropospheric gradients, which provide information on directional changes in atmospheric delay and therefore constrain horizontal moisture variability rather than only the total column moisture amount.

The combined ZTDGRA experiment produces the most distinct redistribution in several sectors. The positive anomaly in the northern sector is enhanced to approximately 11–12 kg m^{-2}, while the positive anomalies from northwest to west are substantially reduced compared with CTRL and ZTD. In the southern sector, the negative anomaly remains pronounced but is weaker than in the ZTD-only experiment. Consequently, adding tropospheric gradients to ZTD does not simply amplify the moisture changes introduced by ZTD assimilation. Instead, it redistributes the moisture anomalies azimuthally, modifying their magnitude differently depending on direction around the cyclone.

These results complement the spatial IWV difference fields shown in Fig. 5. Together, the two diagnostics indicate that ZTD observations strongly constrain the column-integrated moisture field, whereas tropospheric gradients provide additional information on its horizontal organization. The differences between ZTD and ZTDGRA are particularly important in this context: the addition of gradients modifies both positive and negative anomalies around the cyclone rather than uniformly increasing their magnitude. This demonstrates the complementary role of tropospheric gradients in representing the asymmetric moisture environment surrounding Typhoon Koinu.

Such changes in moisture asymmetry may affect the distribution of convection and diabatic heating around the cyclone and, through their interaction with the storm circulation, contribute to changes in the surrounding environmental flow. The following section therefore examines whether the moisture adjustments associated with GNSS assimilation are accompanied by changes in the environmental steering flow.

https://doi.org/10.5194/egusphere-2026-4285
Preprint. Discussion started: 19 August 2026

4.5 Impact on environmental steering flow

To investigate whether moisture adjustments resulting from GNSS observations influence the large-scale circulation surrounding Typhoon Koinu, the environmental steering flow was evaluated throughout the storm evolution. The steering flow was defined as the deep-layer mean horizontal wind averaged between 850 and 500 hPa within a radial annulus extending from 300 to 700 km around the best-track storm center (Section 3). This layer is commonly used in tropical cyclone studies because it represents the vertically averaged environmental circulation that governs the motion of mature tropical cyclones while minimizing the influence of boundary-layer friction and upper-level outflow (Chan and Gray, 1982; Wu and Emanuel, 1995). Likewise, the 300–700 km annulus characterizes the surrounding environmental flow while reducing contamination from the intense inner-core circulation (Carr and Elsberry, 1995). Wind components from the WRF simulations were first interpolated to standard pressure levels and then spatially averaged within the selected annulus. The same procedure was applied to the ERA5 reanalysis, which serves as the reference for evaluating the simulated steering flow. The resulting deep-layer mean wind provides a widely accepted proxy for the environmental steering current controlling tropical cyclone motion.

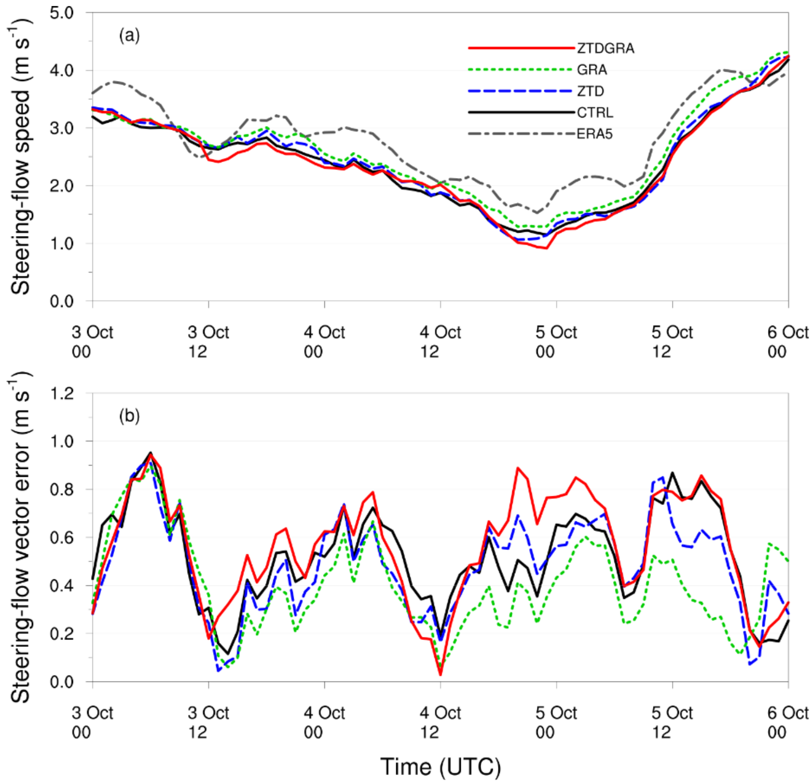

Figure 7 Temporal evolution of the environmental steering flow during the passage of Super Typhoon Koinu from 3 October 2023 00:00 UTC to 6 October 2023 00:00 UTC. The steering flow is defined as the deep-layer mean wind averaged between 850 and 500 hPa within a radial annulus extending from 300 to 700 km around the best-track storm center. (a) Steering-flow wind speed (m s^{-1}) derived from ERA5 and from the CTRL, ZTD, GRA, and ZTDGRA experiments. (b) Steering-flow vector error (m s^{-1}) relative to ERA5 for the four WRF experiments. The assimilation of GNSS observations produces small but systematic changes in the environmental steering flow, with the GRA experiment generally exhibiting the smallest vector errors during the latter part of the simulation, indicating a modest improvement in the representation of the large-scale circulation governing the typhoon motion.

https://doi.org/10.5194/egusphere-2026-4285
Preprint. Discussion started: 19 August 2026

The ERA5 reference steering flow weakened steadily from approximately 3.7 m s⁻¹ on 3 October to about 1.5 m s⁻¹ on 5 October as Typhoon Koinu approached and crossed southern Taiwan (Fig. 7a). Following landfall, the environmental flow strengthened rapidly, exceeding 4 m s⁻¹ by 6 October. This evolution reflects the changing large-scale circulation that controls the storm's motion before, during, and after land interaction.

All WRF experiments successfully reproduce the overall temporal evolution of the steering flow, including the gradual weakening before landfall and the subsequent recovery. However, the simulated steering-flow magnitude is generally weaker than ERA5 throughout much of the analysis period, particularly during the weak-steering phase on 4–5 October. Despite this systematic underestimation, the timing of both the minimum steering flow and the subsequent intensification is well captured. Differences among the assimilation experiments are relatively small in terms of steering-flow magnitude. Nevertheless, the GNSS assimilation experiments generally follow the ERA5 evolution more closely than the CTRL simulation, indicating that the additional moisture information contributes to a more realistic representation of the environmental circulation surrounding the cyclone.

The steering-flow vector errors relative to ERA5 are shown in Fig. 7b. Overall, the errors remain below 1 m s⁻¹ throughout the simulation, demonstrating that the large-scale environmental circulation is reasonably represented in all experiments. However, systematic differences emerged after approximately 4 October 12 UTC, when Typhoon Koinu approached the dense GNSS network over Taiwan.

During this period, all GNSS assimilation experiments generally reduce the steering-flow error relative to the CTRL simulation. The GRA experiment exhibits the smallest vector errors during much of the landfall and post-landfall period, while the ZTD experiment also shows noticeable improvements. The combined ZTDGRA experiment performs similarly to the other GNSS experiments but does not consistently produce the lowest steering-flow error. This behavior suggests that tropospheric gradients primarily improve the horizontal organization of the environmental moisture field, leading to subtle but measurable improvements in the surrounding steering circulation.

Although the differences in steering-flow error are modest, they are consistent with the results presented in Sections 4.3 and 4.4, where assimilating tropospheric gradients modified the spatial and azimuthal distributions of atmospheric moisture by providing additional constraints on horizontal moisture variability. These findings indicate that the influence of GNSS observations on tropical cyclone motion is largely indirect: improvements in moisture analysis modify diabatic heating and the surrounding environmental circulation, which subsequently affect the steering flow that controls storm motion.

The following section examines whether these improvements in the environmental steering flow translate into enhanced forecasts of the typhoon track.

https://doi.org/10.5194/egusphere-2026-4285
Preprint. Discussion started: 19 August 2026

4.6 Impact on typhoon track and intensity prediction

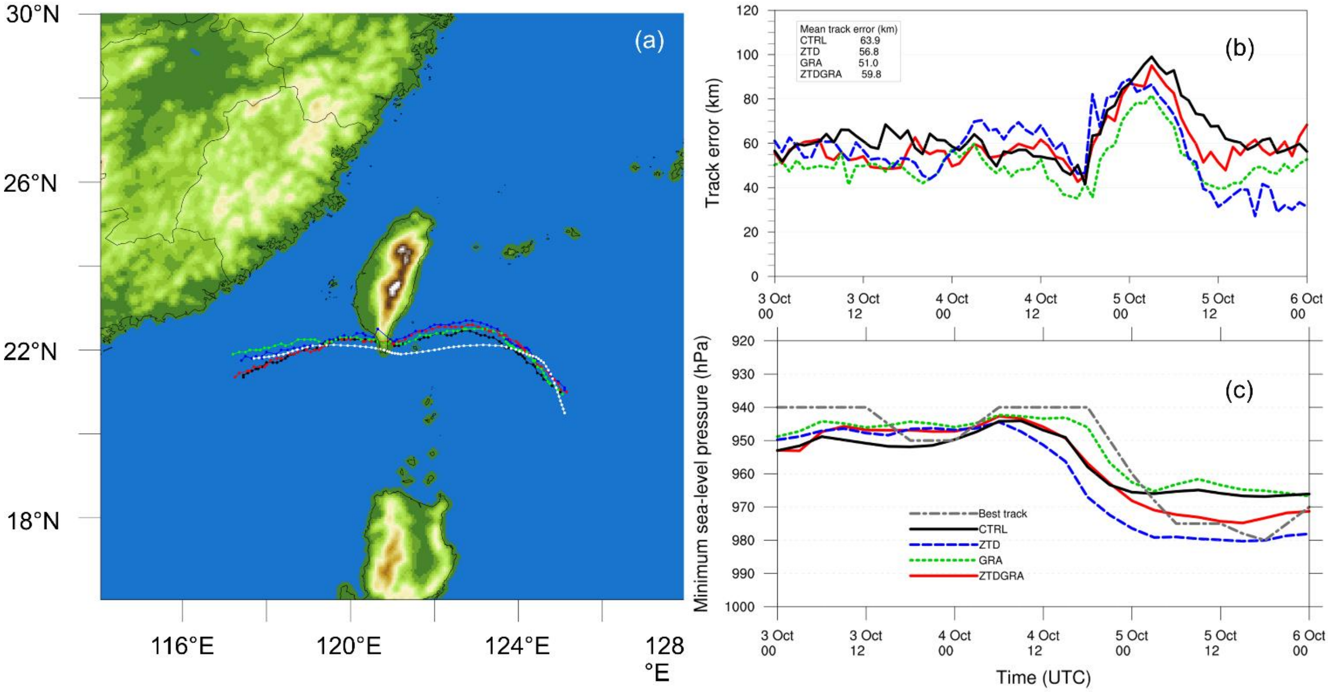

Figure 8 Evaluation of the impact of GNSS data assimilation on the prediction of Super Typhoon Koinu (2023). (a) Simulated typhoon tracks from the CTRL, ZTD, GRA, and ZTDGRA experiments compared with the Joint Typhoon Warning Center (JTWC) best track, shown in white. The experiment tracks use the same colors as those identified in the legend in panel (c). (b) Temporal evolution of the track error, defined as the great-circle distance between the simulated storm center and the JTWC best-track position. Mean track errors over the simulation period are indicated in the inset. (c) Temporal evolution of the minimum sea-level pressure (MSLP) for the four experiments compared with the JTWC best-track MSLP. Assimilation of GNSS observations improves the prediction of the typhoon track, particularly after its interaction with Taiwan. The GRA experiment yields the lowest mean track error, while the combined assimilation of ZTDs and tropospheric gradients (ZTDGRA) provides the best overall representation of the observed MSLP evolution.

The impact of GNSS observations on the simulation of Typhoon Koinu was evaluated by comparing the predicted storm track and minimum sea-level pressure (MSLP) with the Joint Typhoon Warning Center (JTWC) best-track data. The typhoon center in each WRF simulation was identified as the location of the minimum sea-level pressure within a ±3° latitude–longitude search region around the observed storm position. Track error was subsequently calculated as the great-circle distance between the simulated and observed storm centers at each analysis time.

Figure 8a compares the simulated storm tracks from the CTRL, ZTD, GRA, and ZTDGRA experiments with the JTWC best track. All experiments successfully reproduce the overall northwestward movement of Typhoon Koinu toward southern Taiwan and its subsequent westward motion after landfall. During the early stages of the simulation (3–4 October), differences among the experiments are relatively small, indicating that the large-scale steering circulation is already reasonably represented by the model and the assimilated conventional observations.

More pronounced differences emerge as the typhoon approaches and crosses Taiwan. During landfall, the cyclone passes directly over the region containing the highest density of GNSS stations (Fig. 1a), where both ZTDs and tropospheric gradients provide detailed information on the atmospheric moisture field. Following landfall, the GNSS assimilation experiments show a clear correction of the simulated storm trajectory relative to the CTRL experiment, producing tracks that remain closer to the observed best track. This improvement is particularly evident after 5 October, when the CTRL experiment exhibits a greater southward displacement, whereas the GNSS experiments more closely reproduce the observed westward motion toward southeastern China.

The temporal evolution of the track error is shown in Fig. 8b. During the first 36 hours, all experiments maintain relatively small errors, ranging from approximately 50 to 65 km. Around 5 October 00 UTC, the track error increases in all simulations, coinciding with the period when the environmental steering flow reaches its minimum strength (Section 4.5). Under these weak steering conditions, small differences in the environmental moisture distribution and associated diabatic processes can produce noticeable changes in cyclone motion. After this period, the GNSS assimilation experiments recover more rapidly than the CTRL simulation. The GRA experiment achieves the smallest mean track error over the analysis period (51 km), followed by the ZTD experiment (57 km) and the combined ZTDGRA experiment (60 km), compared with 64 km for the CTRL experiment. Although the differences are modest, they consistently indicate that assimilating GNSS observations improves the prediction of cyclone motion.

Figure 8c compares the simulated minimum sea-level pressure with the observed evolution of intensity. All experiments reproduce the gradual weakening of Typhoon Koinu following landfall, including the rapid increase in central pressure associated with the disruption of the cyclone circulation over Taiwan. To quantify the forecast skill, the simulated MSLP was evaluated using the Pearson correlation coefficient, mean absolute error (MAE), and root-mean-square error (RMSE). All experiments show strong temporal agreement with the observations, with correlation coefficients ranging from 0.88 to 0.93. The GRA experiment exhibits the highest correlation with the observed pressure evolution ($r = 0.932$), indicating the most realistic representation of the temporal intensity changes. The combined ZTDGRA experiment provides the smallest absolute pressure errors, yielding an MAE of 5.56 hPa and an RMSE of 7.06 hPa, compared with 7.83 hPa and 8.99 hPa, respectively, for the CTRL experiment. These results indicate that assimilating both ZTDs and tropospheric gradients produces the most accurate overall representation of cyclone intensity.

The improvements in both track and intensity are consistent with the analyses presented in the preceding sections. Assimilation of GNSS observations modifies the horizontal moisture distribution surrounding the cyclone (Section 4.3), leading to a more

https://doi.org/10.5194/egusphere-2026-4285
Preprint. Discussion started: 19 August 2026

realistic representation of the azimuthal moisture asymmetry (Section 4.4). These moisture adjustments are accompanied by small but consistent improvements in the environmental steering flow (Section 4.5), particularly as the steering current weakens near landfall. Together, these changes contribute to a more accurate simulation of both the cyclone trajectory and the evolution of its intensity. Although the improvements are moderate for this individual case, they demonstrate that GNSS tropospheric gradients provide complementary information to ZTDs, enhancing the representation of the storm environment and ultimately improving tropical cyclone prediction.

5. Conclusion

This study investigated the impact of assimilating GNSS ZTDs and tropospheric gradients on the simulation of Super Typhoon Koinu (2023) using the WRF 3DVAR data assimilation system. Four experiments were conducted: a control experiment assimilating conventional observations (CTRL), experiments assimilating either ZTDs (ZTD) or tropospheric gradients (GRA), and a combined experiment assimilating both observation types (ZTDGRA). In addition to the typhoon case study, a two-month assimilation experiment using observations from approximately 250 GNSS stations was conducted to assess the overall impact of these observations across a wide range of meteorological conditions.

The two-month statistical evaluation demonstrates that GNSS observations substantially improve the atmospheric analysis. Assimilation of ZTD observations reduced the ZTD root-mean-square error (RMSE) by approximately 58 %, while the combined assimilation of ZTDs and tropospheric gradients increased the improvement to about 60 %. Importantly, assimilating tropospheric gradients alone reduced the ZTD RMSE by approximately 17 %, demonstrating that gradients contain independent atmospheric information that complements the vertically integrated moisture information provided by ZTDs. Together with previous studies conducted over Europe (Thundathil et al., 2024, 2025), these results confirm that the additional information contained in tropospheric gradients remains beneficial even in the highly moist tropical environment of the western North Pacific.

During Typhoon Koinu, GNSS observations modified the moisture distribution surrounding the cyclone. While ZTD observations primarily adjusted the total atmospheric moisture content, tropospheric gradients improved the representation of the horizontal moisture structure, leading to distinct modifications of the azimuthal moisture asymmetry around the storm. Because these asymmetries influence convective organization and diabatic heating, the improved moisture analysis also led to small but consistent improvements in the environmental steering flow and, consequently, in the simulated typhoon track. The most noticeable improvements occurred after landfall over Taiwan, where the dense GNSS network provided enhanced observational coverage of the cyclone environment. The combined ZTDGRA experiment also produced the lowest sea-level pressure errors, indicating that assimilating both observation types improves not only the surrounding moisture field but also the representation of cyclone intensity.

Although the improvements in steering flow and track prediction are moderate, they are physically consistent with the improved representation of atmospheric moisture demonstrated throughout the analysis. Rather than acting directly on the

https://doi.org/10.5194/egusphere-2026-4285
Preprint. Discussion started: 19 August 2026

wind field, GNSS observations influence the thermodynamic structure of the storm environment, which in turn affects the environmental circulation that governs cyclone motion. This provides a physically coherent pathway linking GNSS moisture observations to improvements in tropical cyclone prediction.

The present study is limited to a single tropical cyclone; additional case studies are required to establish the robustness and statistical significance of the results across different storm characteristics and environmental conditions. Future work should also investigate convection-permitting simulations, where the higher spatial resolution is expected to exploit better the fine-scale horizontal moisture information provided by tropospheric gradients. Extending the assimilation of GNSS tropospheric products to next-generation modeling systems, such as the Model for Prediction Across Scales (MPAS), will further enable evaluation of their impact on regional and global weather prediction.

Overall, this study demonstrates that GNSS tropospheric gradients provide complementary atmospheric information beyond conventional zenith total delay observations. Their assimilation improves the representation of horizontal moisture variability, enhances the analysis of the tropical cyclone environment, and contributes to more accurate simulations of cyclone track and intensity. As dense GNSS networks continue to expand worldwide, tropospheric gradients have strong potential to become a valuable component of future operational numerical weather prediction systems.

Code and data availability

The WRFDA code version 4.4.1, with the gradient operator codes, is available for download. It is stored on Zenodo, a general-purpose open repository developed under the European Open-Access Infrastructure for Research in Europe (OpenAIRE) program and operated by the European Organization for Nuclear Research (CERN). The access link is https://zenodo.org/doi/10.5281/zenodo.13734634.

Author contributions

The original draft of the study was written by RT, who also conducted the formal analysis and experiments. FZ and RT worked together to modify the WRFDA code and develop the gradient operator. Additionally, FZ reviewed the manuscript. TS provided the ECMWF conventional dataset for assimilation, offered relevant scientific input, and also reviewed the manuscript. JW and GD supervised the project, secured funding, and reviewed the paper.

Competing interests

The authors declare that they have no conflict of interest.

https://doi.org/10.5194/egusphere-2026-4285
Preprint. Discussion started: 19 August 2026

Disclaimer

All the maps in the figures were created using Weather Research and Forecasting model simulations.

Acknowledgements

The research project is funded by the German Research Foundation (DFG; grant no. 68510200) and is titled "Exploitation of GNSS tropospheric gradients for severe weather Monitoring And Prediction (EGMAP)." The ECMWF operational analysis was provided by Torsten Schmidt from Section 1.1 Space Geodetic Techniques, GFZ Helmholtz Centre for Geosciences. The authors gratefully acknowledge the Karlsruhe Institute of Technology (KIT) for providing access to the HoreKa High Performance Computing (HPC) system, on which the numerical simulations for the Typhoon Koinu case study were performed. The authors also thank the Nevada Geodetic Laboratory for providing the GNSS tropospheric products used in this study.

Financial support

The research project is funded by the German Research Foundation (DFG; grant no. 68510200) through the project EGMAP.

Review statement

The review statement will be added by Copernicus Publications listing the handling editor as well as all contributing referees according to their status anonymous or identified.

References

Bar-Sever, Y. E., Kroger, P. M., and Borjesson, J. A.: Estimating horizontal gradients of tropospheric path delay with a single GPS receiver, J. Geophys. Res. Solid Earth, 103(B3), 5019–5035, https://doi.org/10.1029/97JB03534, 1998.

Bennitt, G. V., and Jupp, A.: Operational assimilation of GPS zenith total delay observations into the Met Office numerical weather prediction models, Mon. Weather Rev., 140(8), 2706–2719, https://doi.org/10.1175/MWR-D-11-00156.1, 2012.

Bevis, M., Businger, S., Herring, T. A., Rocken, C., Anthes, R. A., and Ware, R. H.: GPS meteorology: Remote sensing of atmospheric water vapor using the global positioning system, J. Geophys. Res. Atmos., 97(D14), 15787–15801, https://doi.org/10.1029/92JD01517, 1992.

Boniface, K., Ducrocq, V., Jaubert, G., Yan, X., Brousseau, P., Masson, F., Champollion, C., Chéry, J., and Doerflinger, E.: Impact of high-resolution data assimilation of GPS zenith delay on Mediterranean heavy rainfall forecasting, Ann. Geophys., 27(7), 2739–2753, https://doi.org/10.5194/angeo-27-2739-2009, 2009.

https://doi.org/10.5194/egusphere-2026-4285
Preprint. Discussion started: 19 August 2026

Brenot, H., Neméghaire, J., Delobbe, L., Clerbaux, N., De Meutter, P., Deckmyn, A., Delcloo, A., Frappez, L., and Van Roozendael, M.: Preliminary signs of the initiation of deep convection by GNSS, Atmos. Chem. Phys., 13(11), 5425–5449, https://doi.org/10.5194/acp-13-5425-2013, 2013.

Caldas-Alvarez, A., and Khodayar, S.: Assessing atmospheric moisture effects on heavy precipitation during HyMeX IOP16 using GPS nudging and dynamical downscaling, Nat. Hazards Earth Syst. Sci., 20(10), 2753–2776, https://doi.org/10.5194/nhess-20-2753-2020, 2020.

Carr III, L. E., and Elsberry, R. L.: Monsoonal interactions leading to sudden tropical cyclone track changes. Monthly Weather Review, 123(2), 265-290, https://doi.org/10.1175/1520-0493(1995)123%3C0265:MILTST%3E2.0.CO;2, 1995.

Chen, F., and Dudhia, J.: Coupling an advanced land surface–hydrology model with the Penn State–NCAR MM5 modeling system. Part I: Model implementation and sensitivity, Mon. Weather Rev., 129(4), 569–585, https://doi.org/10.1175/1520-0493(2001)129%3C0569:CAALSH%3E2.0.CO;2, 2001.

Chan, J. C., & Gray, W. M.: Tropical cyclone movement and surrounding flow relationships. Mon. Weather Rev., 110(10), 1354-1374. https://doi.org/10.1175/1520-0493(1982)110%3C1354:TCMASF%3E2.0.CO;2, 1982.

Davis, J. L., Elgered, G., Niell, A. E., and Kuehn, C. E.: Ground-based measurement of gradients in the "wet" radio refractivity of air, Radio Sci., 28(6), 1003–1018, https://doi.org/10.1029/93RS01917, 1993.

Douša, J., Dick, G., Kačmařík, M., Brožková, R., Zus, F., Brenot, H., Stoycheva, A., Möller, G., and Kaplon, J.: Benchmark campaign and case study episode in central Europe for development and assessment of advanced GNSS tropospheric models and products, Atmos. Meas. Tech., 9(7), 2989–3008, https://doi.org/10.5194/amt-9-2989-2016, 2016.

Dudhia, J.: Numerical study of convection observed during the winter monsoon experiment using a mesoscale two-dimensional model, J. Atmos. Sci., 46(20), 3077–3107, https://doi.org/10.1175/1520-0469(1989)046%3C3077:NSOCOD%3E2.0.CO;2, 1989.

Gendt, G., Dick, G., Reigber, C., Tomassini, M., Liu, Y., and Ramatschi, M.: Near real time GPS water vapor monitoring for numerical weather prediction in Germany, J. Meteorol. Soc. Jpn. Ser. II, 82(1B), 361–370, https://doi.org/10.2151/jmsj.2004.361, 2004.

Giannaros, C., Kotroni, V., Lagouvardos, K., Giannaros, T. M., and Pikridas, C.: Assessing the impact of GNSS ZTD data assimilation into the WRF modeling system during high-impact rainfall events over Greece, Remote Sens., 12(3), 383, https://doi.org/10.3390/rs12030383, 2020.

Grell, G. A., and Freitas, S. R.: A scale and aerosol aware stochastic convective parameterization for weather and air quality modeling, Atmos. Chem. Phys., 14(10), 5233–5250, https://doi.org/10.5194/acp-14-5233-2014, 2014.

Hong, S. Y., Noh, Y., and Dudhia, J.: A new vertical diffusion package with an explicit treatment of entrainment processes, Mon. Weather Rev., 134(9), 2318–2341, https://doi.org/10.1175/MWR3199.1, 2006.

Iacono, M. J., Delamere, J. S., Mlawer, E. J., Shephard, M. W., Clough, S. A., and Collins, W. D.: Radiative forcing by long-lived greenhouse gases: Calculations with the AER radiative transfer models, J. Geophys. Res.-Atmos., 113, D13103, https://doi.org/10.1029/2008JD009944, 2008.

https://doi.org/10.5194/egusphere-2026-4285
Preprint. Discussion started: 19 August 2026

Iwabuchi, T., Miyazaki, S. I., Heki, K., Naito, I., and Hatanaka, Y.: An impact of estimating tropospheric delay gradients on tropospheric delay estimations in the summer using the Japanese nationwide GPS array, J. Geophys. Res. Atmos., 108(D10), https://doi.org/10.1029/2002JD002214, 2003.

Jiménez, P. A., Dudhia, J., González-Rouco, J. F., Navarro, J., Montávez, J. P., and García-Bustamante, E.: A revised scheme for the WRF surface layer formulation, Mon. Weather Rev., 140(3), 898–918, https://doi.org/10.1175/MWR-D-11-00056.1, 2012.

Kačmařík, M., Douša, J., Zus, F., Václavovic, P., Balidakis, K., Dick, G., and Wickert, J.: Sensitivity of GNSS TGs to processing options, Ann. Geophys., 37(3), 429–446, https://doi.org/10.5194/angeo-37-429-2019, 2019.

Lagasio, M., Pulvirenti, L., Parodi, A., Boni, G., Pierdicca, N., Venuti, G., Realini, E., Tagliaferro, G., Barindelli, S., and Rommen, B.: Effect of the ingestion in the WRF model of different Sentinel-derived and GNSS-derived products: analysis of the forecasts of a high impact weather event, Eur. J. Remote Sens., 52(sup4), 16–33, https://doi.org/10.1080/22797254.2019.1642799, 2019.

Li, X., Zus, F., Lu, C., Ning, T., Dick, G., Ge, M., Wickert, J., and Schuh, H.: Retrieving high-resolution tropospheric gradients from multiconstellation GNSS observations, Geophys. Res. Lett., 42(10), 4173–4181, https://doi.org/10.1002/2015GL063856, 2015.

Lindskog, M., Ridal, M., Thorsteinsson, S., and Ning, T.: Data assimilation of GNSS zenith total delays from a Nordic processing centre, Atmos. Chem. Phys., 17(22), 13983–13998, https://doi.org/10.5194/acp-17-13983-2017, 2017.

Mahfouf, J. F., Ahmed, F., Moll, P., and Teferle, F. N.: Assimilation of zenith total delays in the AROME France convective scale model: a recent assessment, Tellus A Dyn. Meteorol. Oceanogr., 67(1), 26106, https://doi.org/10.3402/tellusa.v67.26106, 2015.

Mascitelli, A., Federico, S., Fortunato, M., Avolio, E., Torcasio, R. C., Realini, E., Mazzoni, A., Transerici, C., Crespi, M., and Dietrich, S.: Data assimilation of GPS-ZTD into the RAMS model through 3D-Var: preliminary results at the regional scale, Meas. Sci. Technol., 30(5), 055801, https://doi.org/10.1088/1361-6501/ab0b87, 2019.

Mascitelli, A., Federico, S., Torcasio, R. C., and Dietrich, S.: Assimilation of GPS Zenith Total Delay estimates in RAMS NWP model: Impact studies over central Italy, Adv. Space Res., 68(12), 4783–4793, https://doi.org/10.1016/j.asr.2020.08.031, 2021.

Morel, L., Pottiaux, E., Durand, F., Fund, F., Boniface, K., de Oliveira Junior, P. S., and Van Baelen, J.: Validity and behaviour of TGs estimated by GPS in Corsica, Adv. Space Res., 55(1), 135–149, https://doi.org/10.1016/j.asr.2014.10.004, 2015.

Poli, P., Moll, P., Rabier, F., Desroziers, G., Chapnik, B., Berre, L., Healy, S. B., Andersson, E., and El Guelai, F. Z.: Forecast impact studies of zenith total delay data from European near real-time GPS stations in Météo France 4DVAR, J. Geophys. Res. Atmos., 112(D6), https://doi.org/10.1029/2006JD007430, 2007.

Powers, J. G., Klemp, J. B., Skamarock, W. C., Davis, C. A., Dudhia, J., Gill, D. O., Coen, J. L., Gochis, D. J., Ahmadov, R., Peckham, S. E., Grell, G. A., Michalakes, J., Trahan, S., Benjamin, S. G., Alexander, C. R., Dimego, G. J., Wang, W., Schwartz, C. S., Romine, G. S., Liu, Z., Snyder, C., Chen, F., Barlage, M. J., Yu, W., and Duda, M. G.: The weather research

https://doi.org/10.5194/egusphere-2026-4285
Preprint. Discussion started: 19 August 2026

and forecasting model: Overview, system efforts, and future directions, Bull. Am. Meteorol. Soc., 98(8), 1717–1737, https://doi.org/10.1175/BAMS-D-15-00308.1, 2017.

Skamarock, W. C., Klemp, J. B., Dudhia, J., Gill, D. O., Barker, D. M., Duda, M. G., Huang, X.-Y., Wang, W., and Powers, J. G.: A Description of the Advanced Research WRF Version 3, NCAR Tech. Note, NCAR/TN-475+STR, 113 pp., https://doi.org/10.5065/D68S4MVH, 2008.

Risanto, C. B., Castro, C. L., Arellano, A. F., Moker, J. M., and Adams, D. K.: The impact of assimilating GPS precipitable water vapor in convective-permitting WRF-ARW on North American Monsoon precipitation forecasts over Northwest Mexico, Mon. Weather Rev., 149(9), 3013–3035, https://doi.org/10.1175/MWR-D-20-0394.1, 2021.

Rohm, W., Guzikowski, J., Wilgan, K., and Kryza, M.: 4DVAR assimilation of GNSS zenith path delays and precipitable water into a numerical weather prediction model WRF, Atmos. Meas. Tech., 12(1), 345–361, https://doi.org/10.5194/amt-12-345-2019, 2019.

Singh, R., Ojha, S. P., Puviarasan, N., and Singh, V.: Impact of GNSS signal delay assimilation on short range weather forecasts over the Indian region, J. Geophys. Res. Atmos., 124(17–18), 9855–9873, https://doi.org/10.1029/2019JD030866, 2019.

Thayer, G. D.: An improved equation for the radio refractive index of air, Radio Sci., 9(10), 803–807, https://doi.org/10.1029/RS009i010p00803, 1974.

Thompson, G., Field, P. R., Rasmussen, R. M., and Hall, W. D.: Explicit forecasts of winter precipitation using an improved bulk microphysics scheme. Part II: Implementation of a new snow parameterization, Mon. Weather Rev., 136(12), 5095–5115, https://doi.org/10.1175/2008MWR2387.1, 2008.

Thundathil, R., Zus, F., Dick, G., and Wickert, J.: Assimilation of GNSS tropospheric gradients into the Weather Research and Forecasting (WRF) model version 4.4.1, Geosci. Model Dev., 17(9), 3599–3616, https://doi.org/10.5194/gmd-17-3599-2024, 2024.

Thundathil, R., Zus, F., Dick, G., and Wickert, J.: Assimilation of global navigation satellite system (GNSS) zenith delays and tropospheric gradients: a sensitivity study utilizing sparse and dense station networks, Atmos. Meas. Tech., 18(19), 4907–4922, https://doi.org/10.5194/amt-18-4907-2025, 2025.

Vedel, H., and Huang, X. Y.: Impact of ground based GPS data on numerical weather prediction, J. Meteorol. Soc. Jpn. Ser. II, 82(1B), 459–472, https://doi.org/10.2151/jmsj.2004.459, 2004.

Walpersdorf, A., Calais, E., Haase, J., Eymard, L., Desbois, M., and Vedel, H.: Atmospheric gradients estimated by GPS compared to a high resolution numerical weather prediction (NWP) model, Phys. Chem. Earth A, 26(3), 147–152, https://doi.org/10.1016/S1464-1895(01)00038-2, 2001.

Wickert, J., Dick, G., Schmidt, T., Asgarimehr, M., Antonoglou, N., Arras, C., Brack, A., Ge, M., Kepkar, A., Männel, B., Nguyen, C., Oluwadare, T. S., Schuh, H., Semmling, M., Simeonov, T., Vey, S., Wilgan, K., and Zus, F.:GNSS Remote Sensing at GFZ: Ove: GNSS remote sensing at GFZ: Overview and recent results, ZfV-Z. Geod. Geoinf. Landmanag., (5/2020), https://doi.org/10.12902/zfv-0320-2020, 2020.

https://doi.org/10.5194/egusphere-2026-4285
Preprint. Discussion started: 19 August 2026

Wu, C. C., and Emanuel, K. A.: Potential vorticity diagnostics of hurricane movement. Part 1: A case study of Hurricane Bob (1991). Monthly weather review, 123(1), 69-92, https://doi.org/10.1175/1520-0493(1995)123%3C0069:PVDOHM%3E2.0.CO;2, 1995.

Yan, X., Ducrocq, V., Poli, P., Hakam, M., Jaubert, G., and Walpersdorf, A.: Impact of GPS zenith delay assimilation on convective-scale prediction of Mediterranean heavy rainfall, J. Geophys. Res. Atmos., 114(D3), https://doi.org/10.1029/2008JD011036, 2009.

Yang, S. C., Huang, Z. M., Huang, C. Y., Tsai, C. C., and Yeh, T. K.: A case study on the impact of ensemble data assimilation with GNSS-zenith total delay and radar data on heavy rainfall prediction, Mon. Weather Rev., 148(3), 1075–1098, https://doi.org/10.1175/MWR-D-18-0418.1, 2020.

Zus, F., Balidakis, K., Dogan, A. H., Thundathil, R., Dick, G., and Wickert, J.: DNS (v1.0): An open source ray-tracing tool for space geodetic techniques, Geosci. Model Dev. Discuss., 2025, 1–29, https://doi.org/10.5194/gmd-2024-237, 2025.

Zus, F., Thundathil, R., Dick, G., and Wickert, J.: Fast Observation Operator for Global Navigation Satellite System TGs, Remote Sens., 15(21), 5114, https://doi.org/10.3390/rs15215114, 2023.

Zus, F., Douša, J., Kačmařík, M., Václavovic, P., Dick, G., and Wickert, J.: Estimating the impact of GNSS horizontal delay gradients in variational data assimilation, Remote Sens., 11, 41, https://doi.org/10.3390/rs11010041, 2019.